Cell Stem Cell, Volume *28*

Supplemental Information

Dynamic spatiotemporal coordination of neural stem cell fate decisions occurs through local feedback in the adult vertebrate brain

Nicolas Dray, Laure Mancini, Udi Binshtok, Felix Cheysson, Willy Supatto, Pierre Mahou, Sébastien Bedu, Sara Ortica, Emmanuel Than-Trong, Monika Krecsmarik, Sébastien Herbert, Jean-Baptiste Masson, Jean-Yves Tinevez, Gabriel Lang, Emmanuel Beaurepaire, David Sprinzak, and Laure Bally-Cuif

Dynamic spatiotemporal coordination of neural stem cell fate decisions occurs through local feedback in the adult vertebrate brain

Nicolas Dray[1,*,$], Laure Mancini[1,2,*], Udi Binshtok[3,*], Felix Cheysson[4,5,6,*], Willy Supatto[7], Pierre Mahou[7], Sébastien Bedu[1], Sara Ortica[1], Emmanuel Than-Trong[1,£], Monika Krecsmarik[1], Sébastien Herbert[8,9], Jean-Baptiste Masson[10], Jean-Yves Tinevez[9], Gabriel Lang[4], Emmanuel Beaurepaire[7], David Sprinzak[3,$], Laure Bally-Cuif[1,$,#]

Supplementary figures and legends

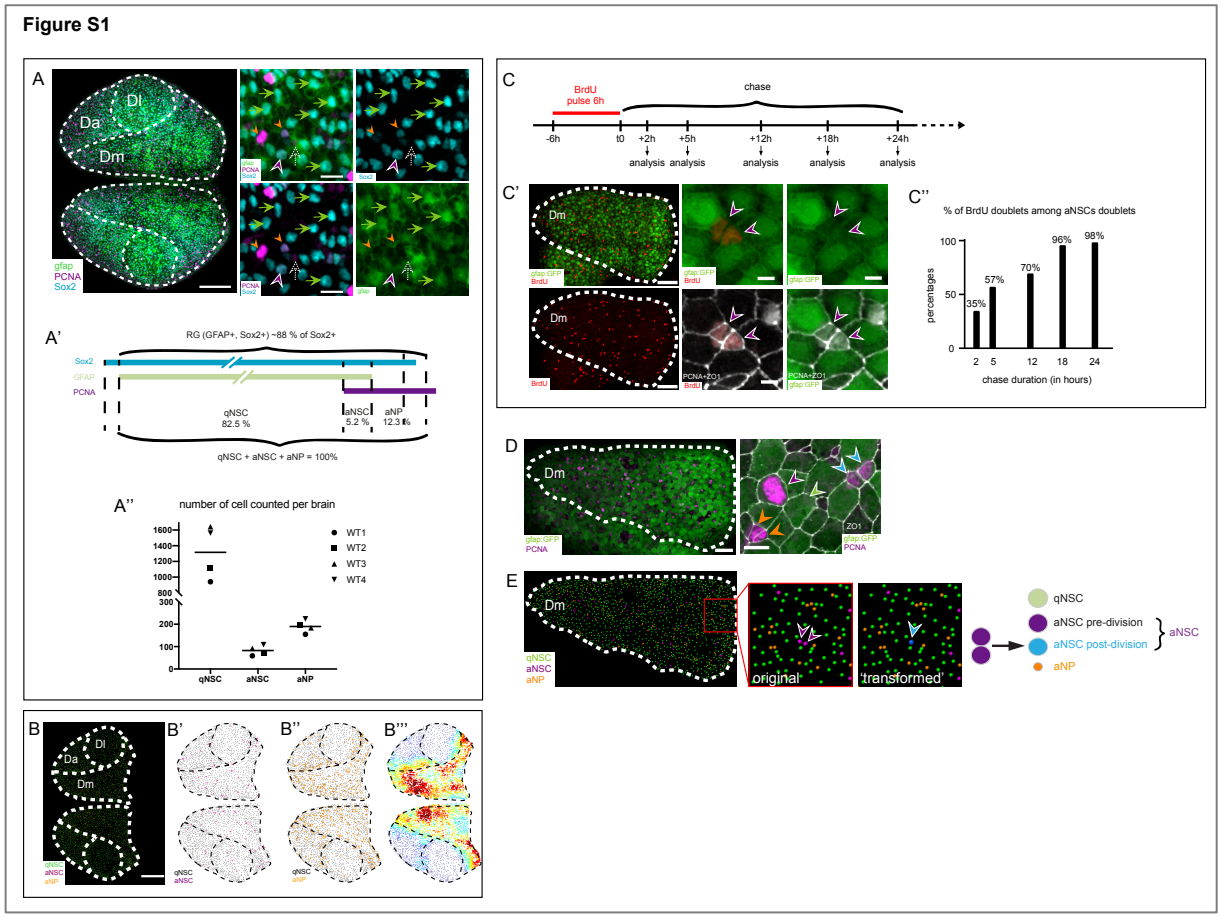

Figure S1. Distribution of pallial progenitors and proliferation states, and identification of aNSC doublets as sister cells post-division, related to Figure 1. (A) Confocal dorsal view of a whole mount adult telencephalon showing the germinal layer of the pallium in a 3mpf *Tg(gfap:GFP)* fish immunostained for GFP (green, NSCs), PCNA (magenta, proliferating cells) and Sox2 (cyan, NSCs + NPs). Anterior is to the left. The pallial neuroanatomical subdivisions (Dl: lateral, Dm: medial, Da: anterior pallial domains) are indicated by dotted lines. Closeups show qNSCs (Sox2+,Gfap+,PCNA-; green arrows), aNSCs (Sox2+,Gfap+,PCNA+; magenta arrowhead), and aNPs (Sox2+,Gfap-,PCNA+; orange

arrowhead). Sox2-,PCNA+ cells (white dotted arrow) are presumably more committed neural progenitors; these cells represent a minority of cell states (Than-Trong et al., 2020a). **(A',A")** Quantitative distribution of progenitor states in Dm, **(A')** based on Sox2 expression and **(A")** plotted from four 3 mpf adult fish (1 hemisphere per fish), from an average, per fish, of 1315 qNSCs (s.e.m =170), 82 aNSCs (s.e.m. =11) and 189 aNPs (s.e.m =14) (as in Figure 1D). **(B-B'')** Semi-automatic cell detection, in the Dm, Da and Dl areas, of the stainings for Sox2 and PCNA (color-coded; magenta cells: Gfap-,PCNA+,Sox2+; orange cells: Gfap-,PCNA+,Sox2-). **(B''')** Local density of the dividing cells (PCNA+ and Sox2+,PCNA+ among all Sox2+ cells) in 50μm-diameter spheres, color-coded from 10% (light blue) to 35% (brown) and where the mean is at 20%. Both hemispheres show a very similar density pattern but the three pallial domains are very different (see also Dray et al., 2015). **(C-C'')** Pulse-chase analysis of BrdU-positive doublets among aNSC doublets following a 6-hour BrdU pulse in a 3mpf *Tg(gfap:GFP)* fish. (C) Experimental scheme. (C') Confocal whole mount dorsal view of the germinal layer of the pallium immunostained for GFP (green), BrdU (red), Sox2 (blue) and PCNA+ZO1 (white, where ZO1 labels apical cell contours), following a 6-hour BrdU pulse and a 18-hour chase. Left: entire views of Dm with focus on BrdU and GFP. Right: closeups from the same brain showing all four markers, with doublet of aNSCs that are also doubly BrdU-positive (magenta/white arrowheads). (C'') Quantification of the proportion of aNSCs doublets where both cells are also BrdU-positive after increasing chase time durations (n=76 aNSCs doublets, from 2 fish). **(D)** Confocal dorsal view of a whole mount adult Dm territory in a 3mpf *Tg(gfap:GFP)* fish immunostained for GFP (green) and PCNA (magenta) and **(D')** closeup of the same sample also showing immunostaining with the Zona Occludens marker ZO1. aNSC singlets (magenta/white arrowhead) are distinguished from doublets (blue/white arrowheads) using the following criteria: proximity of the cell nuclei, similar PCNA staining intensities and similar apical area shape. An aNP singlet is also visible (orange arrowhead). Green arrowhead to a qNSC. **(E)** Cell detection picture of **(D)** highlighting qNSCs (green dots), aNSCs (magenta dots) and aNPs (orange dots). Closeups show the conversion of 2 sister aNSCs (purple arrowheads) into a single post-division aNSC (blue arrowhead) for analysis (see also scheme, right). Scale bars: A (left), B-B''' and C' (left): 100μm; A (right) 15μm; C' (right): 30μm (right); D (left) and E: 50μm; D (right): 10μm. A,C,D,E are stiches of 4 tiles with 10% overlap.

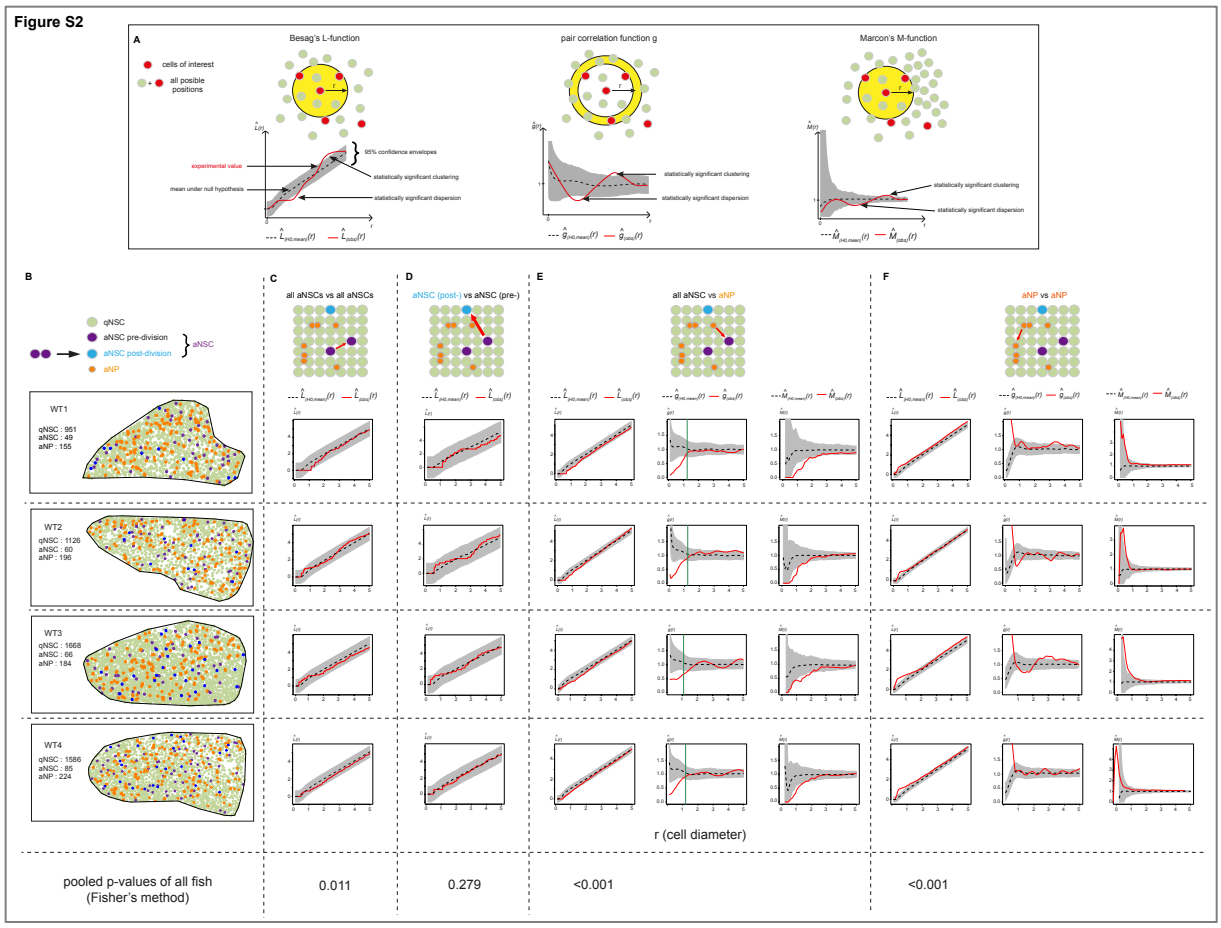

Figure S2. Spatial pattern analysis of NSC activation events in 4 independent wildtype brains, related to Figure 1. (A) Schematics of the principles (top panels) and read-outs (bottom panels) of Besag's *L*-function (Besag, 1977) (left), the pair correlation function *g* (a rescaled derivative of Ripley's K-function) (middle), and the M-function (right) (Marcon and Puech, 2010; Marcon et al., 2012), assessing correlations between the positions of test cells (red dots) relative to each other within a cell ensemble (green and red dots). $L_{(obs)}(r)$, $g_{(obs)}(r)$ and $M_{(obs)}(r)$ (red lines) are experimental values and, $L_{(H0,\ mean)}(r)$, $g_{(H0,\ mean)}(r)$ and $M_{(H0,\ mean)}(r)$ (black dotted lines) are the means under the null hypothesis Random Labelling (RL), i.e. the state of any cell is independent of other cells and independent of its position (Baddeley et al., 2016). *r* will be expressed in cell diameters (where 1 is the mean distance between all the cells). Grey regions are the 95% confidence envelopes under the null hypothesis, separating domains of attraction, randomness and repulsion. In short, the *L*- and *M*-functions count the number of test cells within a circled area of radius *r* around reference cells, while the *g* function only considers test cells within concentric rings at distance *r* of the reference cells, which permits to determine the radius of detected interactions. As the *M*-function is adjusted for the frequency of test cells across the entire Dm domain, it helps determine the strength of the interaction. **(B)** Dm surfaces analyzed for each 3mpf adult pallium (4 hemispheres from 4 wildtype fish (WT1 to WT4) (WT4 is the

same brain as analyzed in Figures 1E and F), with cell states color-coded. Cell numbers are indicated. **(C)** *L*-functions comparing all aNSC activation events (all aNSCs = pre-division + post-division, see scheme in (B)) with each other at the same time point. *r* is the mean cell diameter using the mean distances between all NSCs (qNSC+aNSC) for each Dm surface. aNSC activation events are randomly spaced relative to each other at the same time point in all fish. **(D)** *L*-functions comparing aNSCs post-division with aNSCs pre-division at the same time point. *r* is the mean cell diameter using the mean distances between all cells (qNSC+aNSC+aNP) for each Dm surface. aNSC pre- and post-activation events are randomly spaced relative to each other at the same time point in all fish. **(E)** *L*-, *g*- and *M*-functions showing that activation events (all aNSCs) are consistently dispersed relatively to aNPs. Red and dotted black lines are as in (C), green bars indicate the 95th centile of the distance to the furthest direct neighbor of aNPs. A g-function remaining within the envelope beyond this centile indicates that there is probably no interaction beyond direct neighbors. Reproducibly, NSC activation events are at least two times less likely to occur than predicted by chance within 1-cell diameters from an aNP. **(F)** *L*-, *g*- and *M*-functions showing that aNPs consistently display a clustered pattern at short range (due to the fact that half of them are aNP sister cell doublets, data not shown).

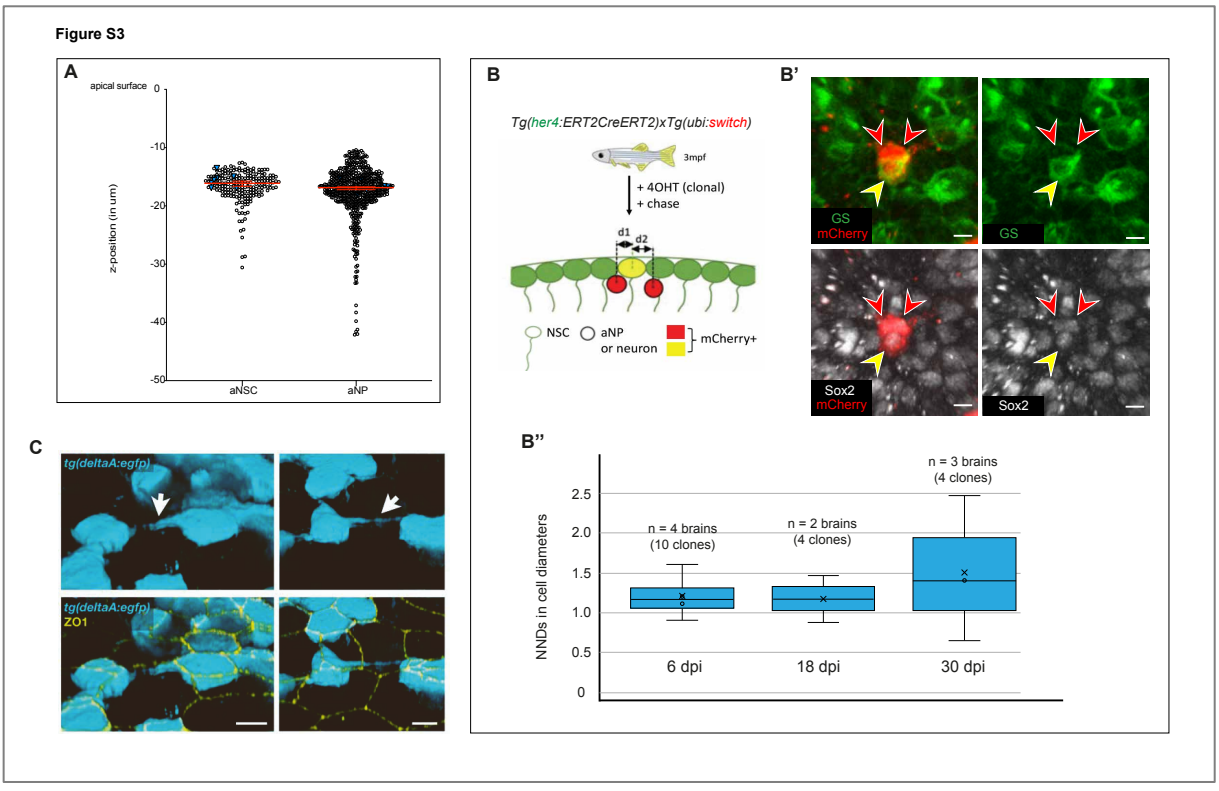

Figure S3. Immunohistological assessment of cell migrations and cell-cell contacts within the adult pallial germinal zone, related to Figures 1 and 2. (A) Position along the z-axis of the center of nuclei, relative to the apical pallial surface (top), for aNSCs (left, n=208) and aNPs (right, n=407) (n=2 brains of 3mpf fish). Blue triangles correspond to aNP-aNSC pairs (one aNSC and one aNP touching each

other). 7 such pairs were found in total. The z-positions of aNP nuclei in such pairs do not differ from those of other aNPs. **(B-B'').** Tracking of NSC-derived clones by mosaic 4-OHT recombination in *Tg(her4:ERT2CreERT2);Tg(ubi:lox-egfp-lox-mCherry)* double transgenic 3mpf adults, and determination of the position of aNPs relative to their mother NSC after a short chase. This procedure reliably tracks individual clones generated by NSCs expressing the marker gene *her4* (equivalent to *gfap* in its distribution) (Than-Trong et al., 2020). (B) Experimental scheme showing, as an example, one 3-cell clone (1 NSC, yellow; 2 aNPs, red) and the measurement of distances (d1, d2) between cell nuclei when projected onto the x,y ventricular plane. (B') Whole-mount confocal view of the germinal tissue after a 6-day chase, immuno-stained for the radial glia marker Glutamine Synthetase (GS), Sox2, and the clonal tracer mCherry (color-coded), showing one 3-cell clone composed of one NSC (GS+,Sox2+,mCherry+, yellow arrow) and two NPs (Sox2+,mCherry+, red arrows). (B'') Tangential nearest neighbor distance (NND) distance separating the nuclei of the NSC and NPs at chase times of 6, 18 and 30 days post-induction (dpi). The data are heteroscedastic hence presented as box and whisker plots. Kruskal-Wallis test: p=0.95. All pairwise comparisons (Behrens Fisher tests): p>0.97. The distances do not vary over time over a duration equivalent to the movies analyzed in our study, and average 1 cell diameter, indicating immediate neighborhood. **(C)** 3D confocal apical views of the morphology of GFP-positive cells (cyan) in the pallial germinal tissue of a 3mpf *Tg(deltaA:egfp)* fish. Top and bottom panels are the same views without and with the ZO1 channel (yellow), respectively. Arrows point to membrane extensions beyond 1 cell diameter. Scale bars: 5µm.

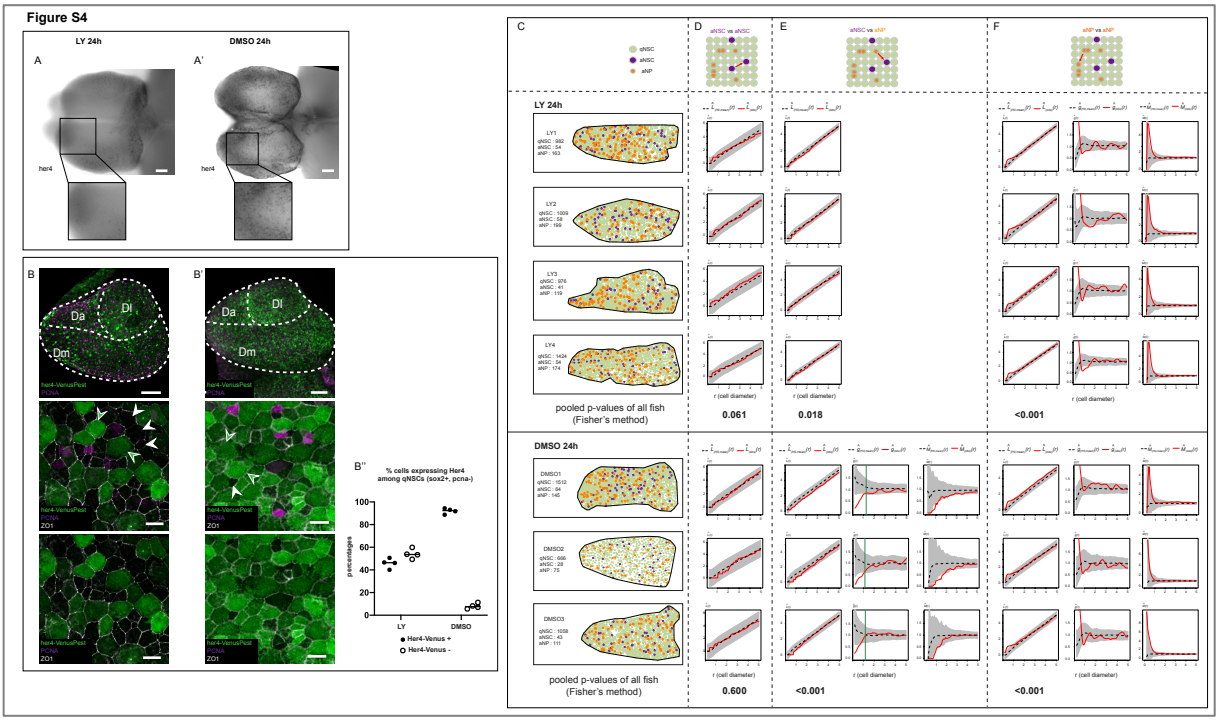

Figure S4. Spatial pattern analysis of NSC activation events upon Notch blockade, related to Figure 2. (A,A') *her4 in situ* hybridization on whole-mount brains showing a strong downregulation upon a 24-hour LY treatment. **(B,B')** Confocal dorsal view of a whole mount adult telencephalon (top) and closeups (bottom), showing the germinal layer of the pallium in a 3mpf *Tg(her4:venusPest)* fish immunostained for Venus (green), PCNA (purple) and ZO1 (white) showing the downregulation of *her4* upon Notch blockade. Examples of qNSCs *her4*-negative (PCNA- with an apical domain, white arrowheads) and *her4*-positive (PCNA- with an apical domain, green arrowheads) are shown. (B) and (B) are stiches of 4 tiles with 10% overlap. (B'') percentages of her4:VenusPEST-positive and her4:VenusPEST-negative cells among qNSCs (Sox2+, PCNA- with an apical domain revealed with ZO1). **(C)** Dm surfaces analyzed for each 3mpf adult pallium (4 hemispheres from 4 fish treated with LY for 24h, 3 hemispheres from 3 fish treated with DMSO), with cell states color-coded. Cell numbers are indicated. In each case, the brain on the top row is the same brain as displayed in Figure 2D. **(D)** *L*-functions (Besag, 1977) comparing aNSC activation events with each other at the same time point, where $L_{(obs)}(r)$ (red lines) are experimental values and $L_{(H0,\ mean)}(r)$ (black dotted lines) are the means under the Random Labelling null hypothesis (CSR). *r* is the mean cell diameter using the mean distances between all cells (qNSC+aNSC+aNP) for each Dm surface. Grey regions are the 95% confidence envelopes. aNSC activation events are randomly spaced relative to each other at the same time point in all fish and this is unchanged upon LY treatment. **(E)** *L*-, *g*- and *M*-functions showing that activation events are consistently dispersed relatively to aNPs in DMSO-treated controls, but that this interaction is abolished upon LY treatment. Red and dotted black lines are as in (D), and green bars indicate the 95th centile of the distance to the furthest direct neighbor of aNPs. A g-function remaining within the envelope beyond this centile indicates that there is probably no interaction beyond direct neighbors. **(F)** *L*-, *g*- and *M*-functions showing that aNPs consistently display a clustered pattern at short range, and that this is unchanged upon LY treatment. Scale bars: A, A': 120µm; B-B': 100µm (top) and 10µm (closeups).

Figure S5

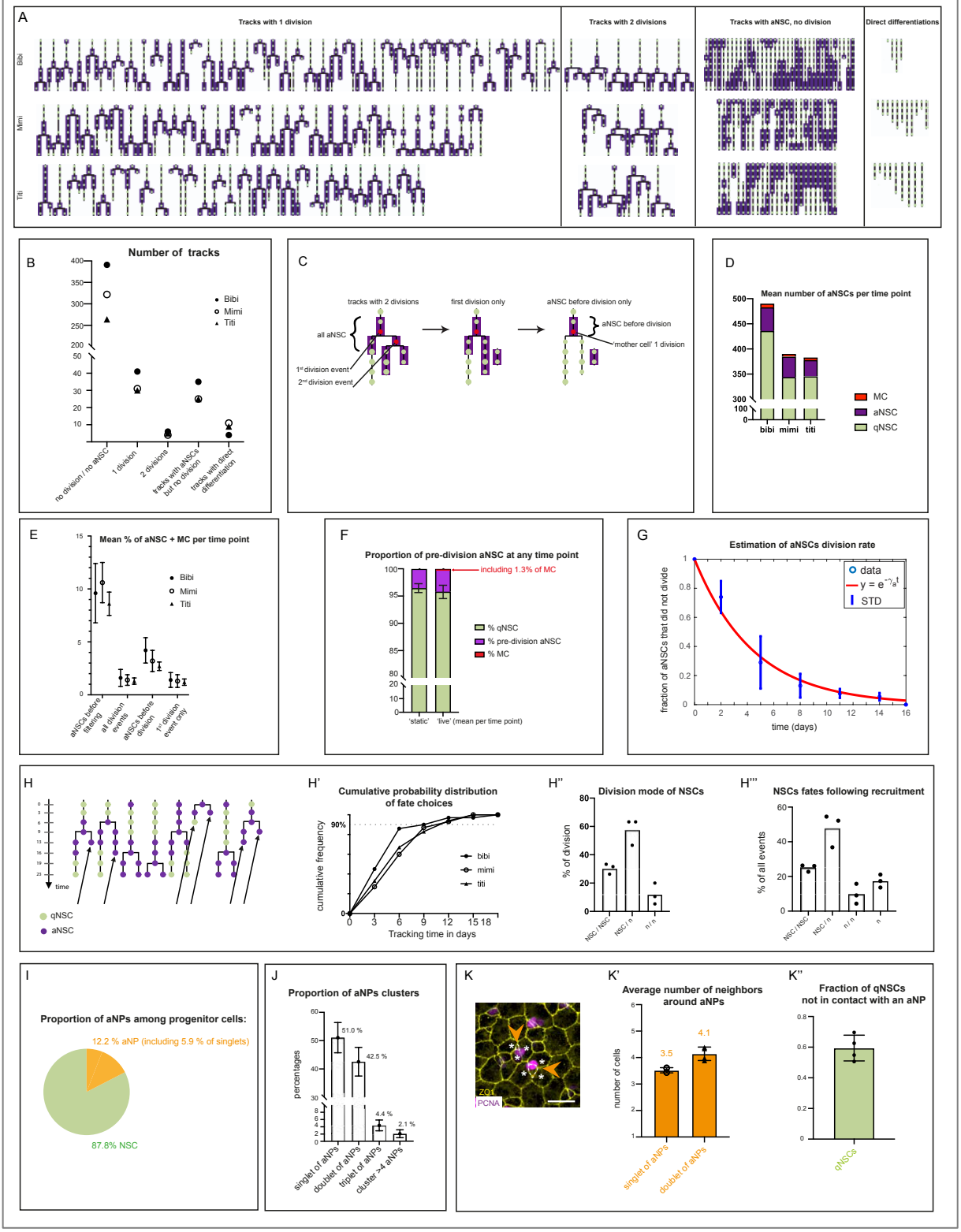

Figure S5. Track categories (except invariable qNSC tracks) in the three adult fish analyzed, related to Figures 3-5, and Experimental parameters implemented into or used to validate the NSC lattice model, related to Figure 6. (A) Representation of all active tracks (i.e. either including (a) division(s) event(s) -1st and 2nd columns- or an activation phase -3rd column- or a direct neuronal differentiation

-4th column-, in the Dm pallial area of the three fish analyzed (Bibi, Mimi and Titi - further illustrated in Figure 3 and Video S1). Bibi and Mimi are re-analyses of (Than-Trong et al., 2020) incorporating the *mcm5:egfp* staining, and Titi is a new animal. Tracks are color-coded (green: qNSC, purple: aNSC) and shown over time from top to bottom (dots are imaging time points, separated by 3 days). **(B)** Quantitative summary of (A). There is a total of 977 qNSC tracks, 99 tracks with 1 division event, 14 with 2 division events, 85 tracks with at least one activated aNSC but no division and 24 tracks losing an NSC through direct differentiation. The total number of NSCs in the tracked population is stable (the numbers of NSCs at the first and last informative time points of the movies were similar: 1285 and 1287 NSCs, respectively). **(C)** Nomenclature and method for the analysis of dividing tracks, color-coded. The "mother cell" (MC in red) is the aNSC at the time point preceding division. To focus on aNSCs before division and on first activation events, we filtered the case of consecutive divisions (only the first division event is considered) and converted all aNSCs post-division to a qNSC state. **(D)** Number of tracks of each state per fish. **(E)** Mean number of NSCs per time point, per fish: ''aNSCs before filtering'': 9.6% (s.e.m. 0.6%), ''division events'': 1.4% (s.e.m. 0.1%), activation events (''aNSCs before division''): 3.4% (s.e.m. 0.2%), ''first division events'': 1.3% (s.e.m. 0.1%). **(F)** Proportion of pre-division activated NSCs at any time point, estimated from the number of aNSC 'singlets' (immunostaining experiments, see Figure S1) and from the average number of pre-division aNSCs per time step (live imaging experiments, see (E). From the latter we could also estimate that the average number of dividing NSC per time point (mother cells -MCs-) is 1.3% (s.e.m. 0.1%). **(G)** Estimation of aNSC activation rate (γ_a). The fraction of remaining aNSCs before division obtained from 88 NSC tracks (blue circles and bars are the average and STD from the 3 fish, respectively) was fitted to a decaying exponential curve (red). The best fit for the activation rate is $\gamma_a = 0.22\ day^{-1}$ with $(0.20\ , 0.25)$ 95% confidence interval. **(H)** Determination of the frequency of each division mode, inferred as in (Than-Trong et al., 2020). Symmetric gliogenic divisions produce two NSCs (NSC/NSC), symmetric neurogenic divisions (n/n) produce two aNPs (future neurons, n) that disappear from the germinal sheet, and asymmetric divisions produce one NSC and one aNP (NSC/n). First, to determine the time needed for NSC fates to become apparent, we focused on the most unambiguous fate accessible, i.e. the loss of an NSC during the imaging (black arrow). This is due to the loss of the expression of *gfap* (there is almost no cell death nor cell migration (Alunni et al., 2013; Dray et al., 2015; Than-Trong et al., 2020). **(H')** Cumulative probability distribution of the time between division and 'fate choice' (=loss of *gfap* expression) showing that 90% of neurogenic fates is resolved by 9 days after division for Bibi and 12 days after division for Mimi and Titi. Thus, to estimate division mode we only considered tracks with at least 9 days after division for Bibi and 12 days after division for Mimi and Bibi. **(H'')** Following 53 such tracks, we could estimate that 30.4% (± s.e.m 2.1%) of division events produce two qNSC, 58% (± s.e.m 5.5%) of division events are asymmetric in fate, and 11.9% (± s.e.m 4.3%) of division events have a symmetric

neurogenic fate (producing neurons and/or aNPs) (cell fates post-division indicated on the x axis). **(H’’’)** Similarly, considering tracks with a direct differentiation happening at least 9 to 12 days after the first time point, we counted 11 direct differentiations. Thus, we could estimate the relative proportions of NSC fates following NSC recruitment (division or direct differentiation) and show that direct differentiations account for 17% (± s.e.m 2.1%) of all events, balancing the gain and loss of NSCs through division (25% (± s.e.m 1.1%) NSC gains via symmetric gliogenic divisions, 9.7% (± s.e.m 5.7%) NSC losses via neurogenic divisions) (similar to Than-Trong et al., 2020). **(I)** Proportion of aNPs among all progenitor cells in Dm, revealed by immunostaining experiments (12.25%, ± s.e.m 1.02%). Among these, about half are present as singlets and half as doublets of aNPs. **(J)** Proportion of aNPs identified as singlets, doublets, triplets or clusters of 4 or more cells (using similar criteria than for the identification of aNSC doublets: similar PCNA staining intensities and similar apical area shape) showing that singlets and doublets of aNPs represent more than 93% of all aNPs. **(K-K’’)** Number of neighbors around singlets and doublets of aNPs, and proportion of qNSCs that do not contact an aNP. (K) The image shows an example of two aNP singlets (orange, arrow) in contact through edges with 3 qNSCs each (asteriscs). (K’) Average number of neighbors for singlets and doublets of aNPs (respectively 3.52 ± s.e.m 0.05%, and 4.14 ± s.e.m 0.13%), revealed using immunostainings for ZO1 (yellow) and PCNA (magenta) on four WT fish (segmented in Figure S3B). (K’’) Proportion of qNSCs among all qNSCs that are not in contact with any aNPs (60% ± s.e.m 5%). Scale bar in K: 10μm.

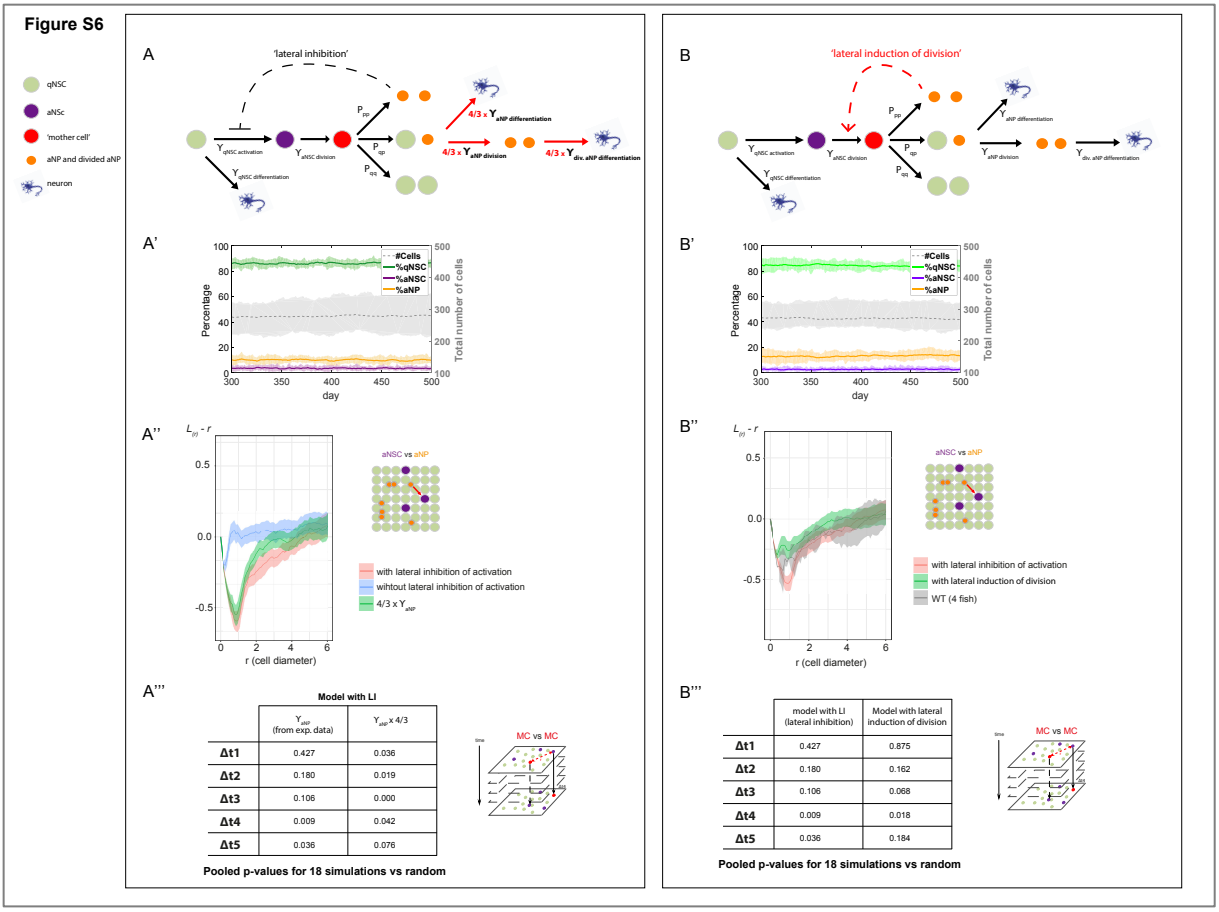

Figure S6. Alternative models assessing the effect of changes in aNPs lifetime or in aNP-mediated regulation on the outcome of the NSC lattice model, related to Figures 6 and 7. (A-A'''') Analysis of a model with shorter aNP lifetime. (A) Schematic of a model where aNP lifetime is reduced by 25% (the aNP rate of division and differentiation is multiplied by 4/3). (A') The model in (A) shows a stable cell numbers and proportions of each cell type over time (results from 18 simulations). (A'') Compared *L*-functions testing the dispersion between aNSCs and aNPs under three modeling conditions: (i) with LI and experimental (default) aNP half-life (pink), (ii) without LI but with experimental (default) aNP half-life (blue), and (iii) the alternative model shown in (A), i.e. with LI and 25% shorter aNP half-life (green) (centered (*L(r)* – *r*) to highlight differences with their 95% confidence intervals, shaded). A similar dispersion is obtained with the two models including LI ((i) and (iii)). (A''') Combined p-values (Fisher's method) of *L*-functions assessing the spatial interaction of MCs relative to each other at all Δt intervals (as in Figures 5 and 7) for the two models including LI ((i): left, (iii)= right) (results from 18 simulations for each model). The two models show a dispersion a Δt4 and Δt3, respectively. **(B-B''')** Analysis of a model encoding an aNP-derived feedback that enhances the division rate of neighboring aNSCs. (B) Schematic representation of the model with a lateral induction of division (dashed red arrow). (B') The model in (B) shows a stable cell numbers and proportions of each cell type over time (results from 18

simulations). (B'') *L*-functions testing the dispersion between aNSCs and aNPs under two modeling conditions: (i) lateral inhibition of qNSC activation (our default model in Figure 6A) (pink) and (ii) lateral induction of aNSC division (green) (18 simulations each), compared with data from wild-type fish (gray) (4 fish, data from Figure S3E) (centered (*L(r)* – *r*) to highlight differences with their 95% confidence intervals, shaded). (B''') Combined p-values (Fisher's method) of *L*-functions assessing the spatial interaction of MCs relative to each other at all Δt intervals (as in Figures 5 and 7) in models (i) and (ii) (results from 18 simulations in each model). Cut-off for pooled *p*-values in A''' and B''' = 0.01.

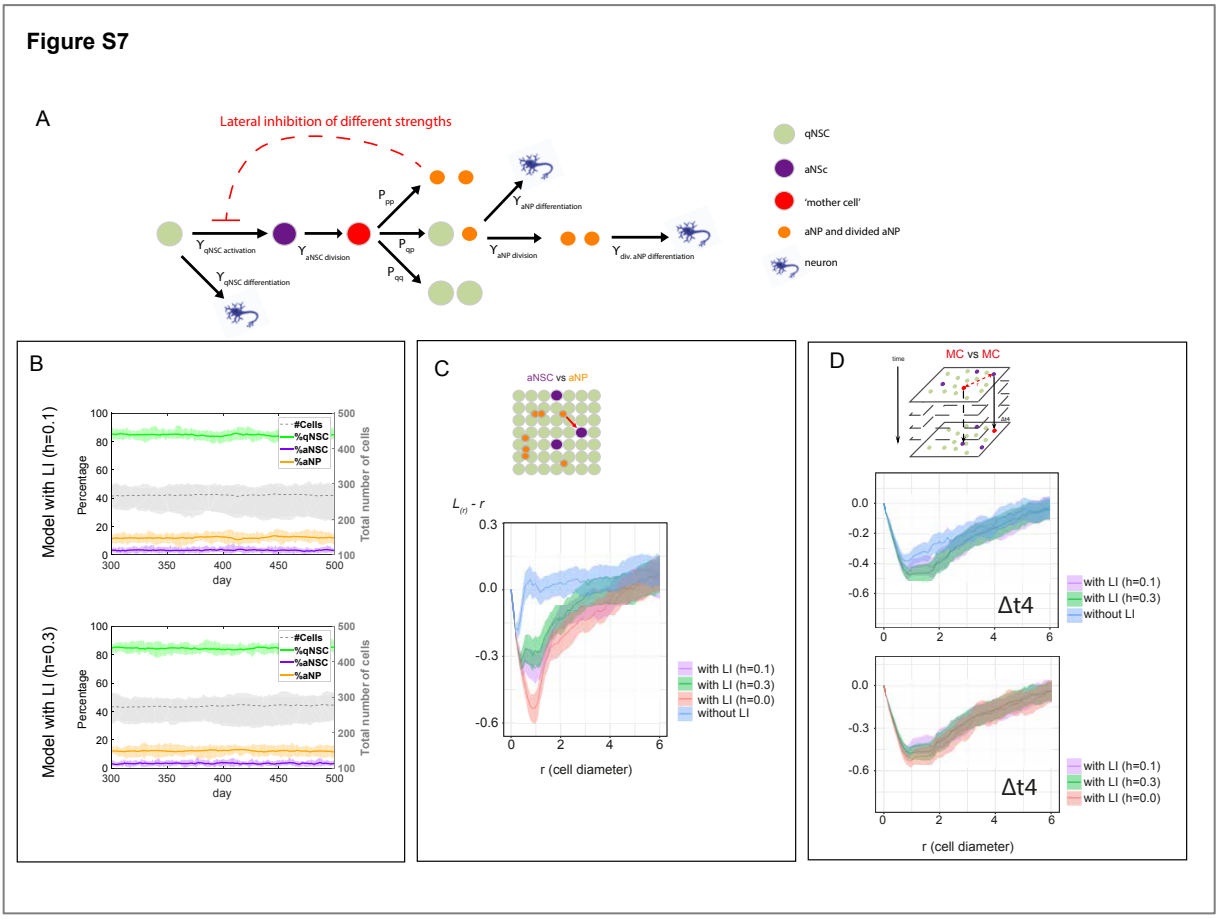

Figure S7. Analysis of the effect of incomplete lateral inhibition of aNP on aNSC activation, related to Figures 1 and 5-7. (A) Schematic of a model where LI from aNPs reduces the activation of neighboring aNSCs, yet the inhibition is not complete. We compare two models where the probability for activation event of qNSC is reduced by 70% ($h = 0.3$) and 90% ($h = 0.1$) when in contact with an aNP (see function h in Figure S8A, right, and equation (30) in the methods). **(B)** Both models in (A), with $h = 0.1$ and $h = 0.3$, show stable cell numbers and proportions of each cell type over time (results from 18 simulations for each model). Note that the inhibition factor $I^{\star}$ was adjusted to generate the stability: $I^{\star} = 0.713$ for the model with $h = 0.3$ and $I^{\star} = 0.631$ for the model with $h = 0.1$ **(C)** Compared *L*-functions testing the dispersion between aNSCs and aNPs under four modeling

conditions: (i) complete LI ($h = 0$) (pink), (ii) incomplete LI with $h = 0.3$ (green), (iii) incomplete LI with $h = 0.1$ (purple), and (iv) without LI (blue) (centered (*L(r) – r*) to highlight differences with their 95% confidence intervals, shaded). A similar dispersion between aNSC and aNP is obtained, but it is weaker as the strength of LI decreases. **(D)** Compared *L*-functions (lines) and their 95% confidence intervals (shaded) testing for dispersion between MCs at Δt4 in the four models in (C) (same color code). All conditions result in a delayed MC dispersion, as observed in vivo, but the effect is slightly weaker as the strength of LI decreases.

Methods supplementary figure and legend

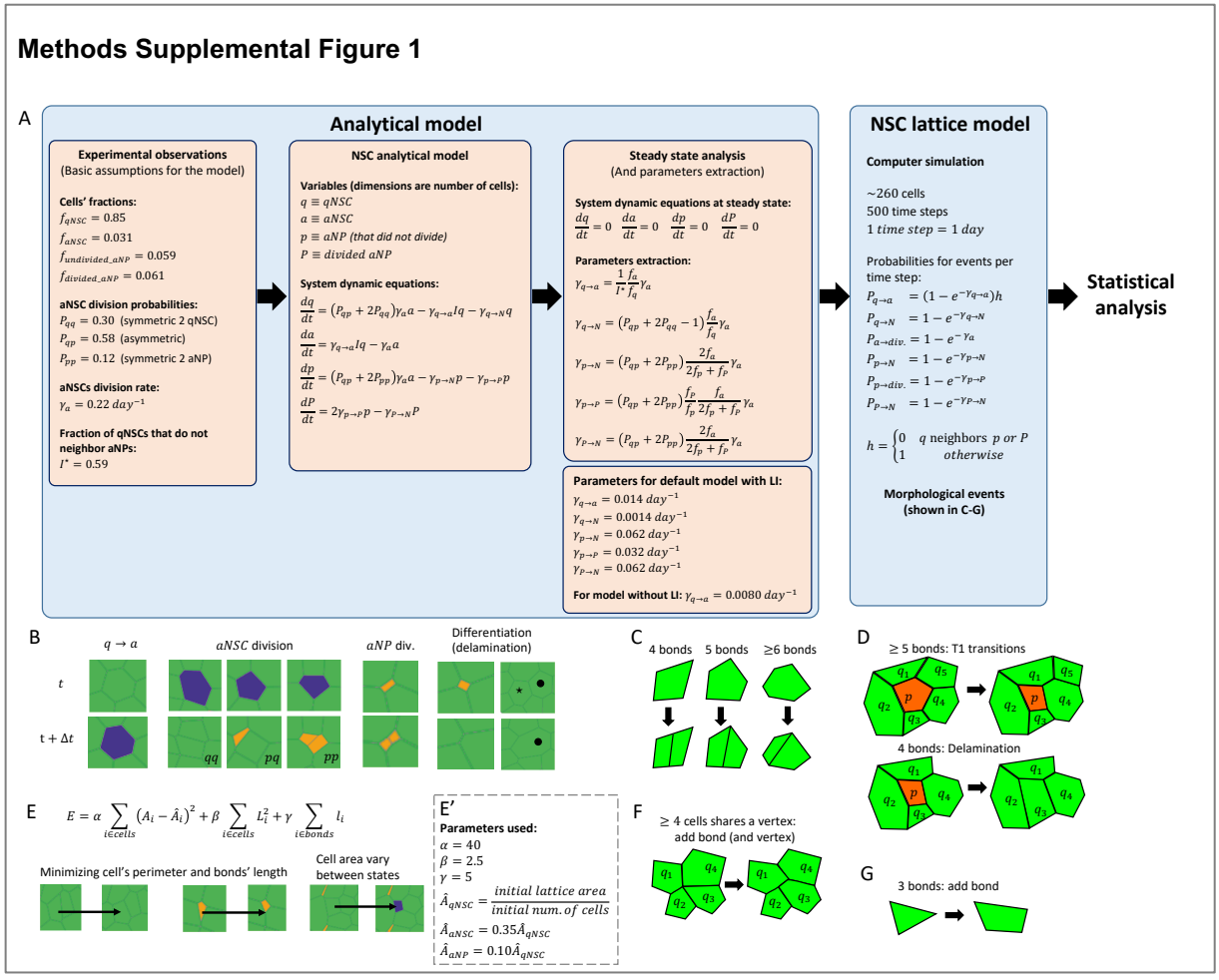

Methods Figure S1. Modeling workflow and description of cell fate transition rules in the NSC lattice model, related to STAR Methods and related to Figures 6 and 7. (A) Scheme showing the main steps and parameters of the model (see methods for details). The two layers of the model include the analytical model (left rectangle) and the NSC lattice model (right rectangle). The analytical model uses as input the experimentally measured values (left inset). The possible transitions in a mean field model are described by the rate equations in the center inset. Steady state analysis which allows estimation

of the transition rates is in the right inset (the rate values for a model with LI and a model without LI are given in the bottom right inset). **(B)** Examples of simulated transitions in two consecutive time steps. **(C)** Schematic of cell division rules. Cell division is carried differently for different cells, depending on the number of bonds in the cell. The division rules are designed so that the daughter cells remain with at least 4 bonds after division (see Methods). **(D)** Schematic of a cell delamination process. Cell delamination occurs in two stages: If the cell has 5 or more bonds it reduces its bonds using T1 transition processes (neighbor exchange) until it is left with 4 bonds, only then it delaminates in a way that reduces the minimum amount of bonds in the surrounding cells. The delamination reduces bonds from surrounding cells with 5 or more bonds. Both (C) and (D) are important for proper maintenance of the simulated tissue. **(E)** Examples of cell morphology changes associated with minimization of the lattice mechanical energy, E. The mechanical energy depends on 3 terms: cell area (unique area for each cell state, A_i), cell perimeter (L_i), and bond length (l_i). **(E')** Parameters of the terms in the energy function given in (E) (See also description in the methods). **(F,G)** Additional morphological corrections are required for long term maintenance of the cell lattice. (F) A new bond (and vertex) is added if a vertex shares more than 3 cells. (G) A new bond is added to a cell with 3 bonds.

Supplementary Tables and legends

Table S1. Cell types and counts used in the static in vivo analysis, related to Figures 1-2.

All aNSCs						% among : qNSC + aNSC + aNP			% among : qNSC + aNSC	
All aNSCs	Among Sox2+ cells only	# qNSC	#aNSC	# aNP	Total number of cells	% aNSC	% aNP	% qNSC	% aNSC	% qNSC
WT	WT1	941	59	155	1155	5.11	13.42	81.47	5.90	94.10
	WT2	1116	70	196	1382	5.07	14.18	80.75	5.90	94.10
	WT3	1643	92	184	1919	4.79	9.59	85.62	5.30	94.70
	WT4	1562	109	224	1895	5.75	11.82	82.43	6.52	93.48
	Average WT	**1315.50**	**82.5**	**189.75**	**1587.75**	**5.18**	**12.25**	**82.57**	**5.91**	**94.09**
	std	**340.62**	**22.37**	**28.59**	**380.23**	**0.41**	**2.03**	**2.15**	**0.50**	**0.50**
	s.e.m	**170.31**	**11.38**	**14.30**	**190.12**	**0.20**	**1.02**	**1.07**	**0.25**	**0.25**
LY 24h	LY1	938	98	163	1199	8.17	13.59	78.23	9.46	90.54
	LY2	977	90	99	1166	7.72	8.49	83.79	8.43	91.57
	LY3	946	71	119	1136	6.25	10.48	83.27	6.98	93.02
	LY4	1344	134	174	1652	8.11	10.53	81.36	9.07	90.93
	Average WT	**1051.25**	**98.25**	**138.75**	**1288.25**	**7.56**	**10.77**	**81.66**	**8.49**	**91.51**
	std	**195.89**	**26.39**	**35.59**	**243.86**	**0.90**	**2.11**	**2.52**	**1.09**	**1.09**
	s.e.m	**97.95**	**13.19**	**17.80**	**121.93**	**0.45**	**1.05**	**1.26**	**0.54**	**0.54**
DMSO 24h	DMSO1	1484	92	145	1721	5.35	8.43	86.23	5.84	94.16
	DMSO2	644	50	75	769	6.50	9.75	83.75	7.20	92.80
	DMSO3	1016	85	111	1212	7.01	9.16	83.83	7.72	92.28
	Average WT	**1048.00**	**75.67**	**110.33**	**1234.00**	**6.29**	**9.11**	**84.60**	**6.92**	**93.08**
	std	**420.91**	**22.50**	**35.00**	**476.38**	**0.85**	**0.67**	**1.41**	**0.97**	**0.97**
	s.e.m	**243.01**	**12.99**	**20,21**	**275.04**	**0.49**	**0.38**	**0.81**	**0.56**	**0.56**

Table S1. Cell states and counts used in the static in vivo analysis, related to Figures 1-2.

Raw numbers of cells counted per fish (1 hemisphere per animal, within the Dm subregion of the pallium only). Cells were classified as qNSCs (Sox2+, Gfap+), aNSC (Sox2+, Gfap+, PCNA+) or aNP (Sox2+, PCNA+). The last three columns are showing the relative proportions of each cell state within the entire Sox2+ population.

Table S2. Cell types and counts used in the dynamic in vivo analysis, related to Figures 3-5.

before filtering (see Figure S5E)						
time point	**# qNSC**	**# aNSC**	**# MC**	**% qNSC**	**% aNSC**	**% MC**
t1	1131	89	17	92.7	7.3	1.4
t2	1133	99	12	92.0	8.0	1.0
t3	1131	106	16	91.4	8.6	1.3
t4	1131	115	16	90.8	9.2	1.3
t5	1129	120	17	90.4	9.6	1.4
t6	1112	142	27	87.7	11.3	2.2
t7	1113	153	21	87.9	12.1	1.7
t8	n/a	n/a	n/a	n/a	n/a	n/a
Sum all t	**7880**	**824**	**126**			
Mean per t	**1125.7**	**117.7**	**18.0**	**90.6**	**9.4**	**1.4**
std	**9.1**	**22.9**	**4.8**	**1.7**	**1.7**	**0.4**
s.e.m	**3.4**	**8.7**	**1.8**	**0.7**	**0.7**	**0.1**

after filtering (see Figure S5E)						
time point	**# qNSC**	**# aNSC**	**# MC**	**% qNSC**	**% aNSC**	**% MC**
t1	1183	37	17	97.0	3.0	1.4
t2	1199	33	11	97.3	2.7	0.9
t3	1119	38	15	96.9	3.1	1.2
t4	1209	37	16	97.0	3.0	1.3
t5	1204	45	14	96.4	3.6	1.1
t6	1197	57	24	95.5	4.5	1.9
t7	1216	50	15	96.1	3.9	1.2
t8	n/a	n/a	n/a	n/a	n/a	n/a
Sum all t	**8407**	**297**	**112**			
Mean per t	**1201.0**	**42.4**	**16.0**	**96.6**	**3.4**	**1.3**
std	**10.4**	**8.6**	**4.0**	**0.7**	**0.7**	**0.3**
s.e.m	**3.9**	**3.3**	**1.5**	**0/2**	**0.2**	**0.1**

Table S2. Cell states and counts used in the dynamic in vivo analysis, related to Figures 3-5.

Raw numbers of the sum of cells counted for the three fish Mimi, Bibi and Titi (1 hemisphere per animal, within the Dm subregion of the pallium only) before (top table) and after (bottom table) filtering (See Figure S5E). The last three columns are showing the relative proportions of each cell state within the qNSC + aNSC population.